Spatially dependent Intensity-Duration-Frequency curves to support the design of civil infrastructure systems

Phuong Dong Le[1,2], Michael Leonard[1], Seth Westra[1]

[1]School of Civil, Environmental and Mining Engineering, University of Adelaide, Adelaide, South Australia, Australia

[2]Thuyloi University, Hanoi, Vietnam

Email: lephuongdong_tb@tlu.edu.vn

Keywords: areal reduction factor, asymptotic independence, conditional probability, duration dependence, extreme rainfall, flood probability, inverted max-stable process, joint probability, spatially dependent Intensity-Duration-Frequency,

Abstract

Conventional flood risk methods typically focus on estimation at a single location, which is inadequate for civil infrastructure systems such as road or railway infrastructure. This is because rainfall extremes are spatially dependent, so that to understand overall system risk it is necessary to assess the interconnected elements of the system jointly. For example, when designing evacuation routes it is necessary to understand the risk of one part of the system failing given that another region is flooded or exceeds the level at which evacuation becomes necessary. Similarly, failure of any single part of a road section (e.g., a flooded river crossing) may lead to the wider system's failure (i.e. the entire road becomes inoperable). This study demonstrates a spatially dependent Intensity-Duration-Frequency curve framework that can be used to estimate flood risk across multiple catchments, accounting for dependence both in space and across different critical storm durations. The framework is demonstrated via a case study of a highway upgrade, comprising five bridge crossings where the upstream contributing catchments each have different times of concentration. The results show that conditional and unconditional design flows can differ by a factor of two, highlighting the importance of taking an integrated approach. There is also a reduction in the failure probability of the overall system compared with the case of no spatial dependence between storms. The results demonstrate the

potential uses of spatially dependent Intensity-Duration-Frequency curves and suggest the need for more conservative design estimates to take into account conditional risks.

1. Introduction

Methods for quantifying the flood risk of civil infrastructure systems such as road and rail networks require considerably more information compared to traditional methods that focus on flood risk at a point. For example, the design of evacuation routes requires the quantification of the risk that one part of the system will fail at the same time that another region is flooded or exceeds the level at which evacuation becomes necessary. Similarly, a railway route may become impassable if any of a number of bridges are submerged, such that the 'failure probability' of that route becomes some aggregation of the failure probabilities of each individual section. Successful estimation of flood risk in these systems therefore requires recognition both of the networked nature of the civil infrastructure system across a spatial domain, as well as the spatial and temporal structure of flood-producing mechanisms (e.g. storms and extreme rainfall) that can lead to system failure (e.g., Leonard et al. (2014), Seneviratne et al. (2012), Zscheischler et al. (2018)).

One way to estimate such flood probabilities is to directly use information contained in historical streamflow data. For example, annual maximum streamflow at two locations might be assumed to follow a bivariate generalized extreme value distribution (Favre et al., 2004; Wang, 2001; Wang et al., 2009), which can then be used to estimate both conditional probabilities (e.g. the probability that one river is flooded given that the other river level exceeds a specified threshold) and joint probabilities (e.g. the probability that one or both rivers are flooded). Several frameworks have been demonstrated based directly on streamflow observations, including functional regression (Requena et al., 2018), multisite copulas (Renard and Lang, 2007), and spatial copulas (Durocher et al., 2016). However, this paper focuses on rainfall-based methods, as in many instances continuous streamflow data are unavailable or insufficient at the locations of interest, or the catchment conditions have changed such that historical streamflow records as unrepresentative of likely future risk.

To overcome common limitations of streamflow data, rainfall-based approaches are commonly used. One method uses continuous rainfall data (either historical or generated) to compute continuous streamflow data using a rainfall-runoff model (Boughton and Droop, 2003; Cameron et al., 1999; He et al., 2011; Hegnauer et al., 2014; Pathiraja et al., 2012), with flood risk then estimated based on the

simulated streamflow time series. This method is computationally intensive and given the challenge of reproducing a wide variety of statistics across many scales, can have difficulties in modelling the dependence of extremes. Most rainfall models operate at the daily timescale (Bárdossy and Pegram, 2009; Baxevani and Lennartsson, 2015; Bennett et al., 2016b; Hegnauer et al., 2014; Kleiber et al., 2012; Rasmussen, 2013), whereas many catchments respond at subdaily timescales. The capacity of space-time rainfall models to simulate the statistics of sub-daily rainfall remains a challenging research problem (Leonard et al., 2008). One approach is to exploit the relative abundance of data at the daily scale, then apply a downscaling model to reach subdaily scales (Gupta and Tarboton, 2016). Continuous simulation is receiving ongoing attention and increasing application, yet there remain limitations when applying these models in many practical contexts.

A second rainfall-based approach proceeds by applying probability calculations on rainfall, to construct 'Intensity-Duration-Frequency' (IDF) curves, which are then translated to a runoff event of equivalent probability via either empirical models such as the rational method to estimate peak flow rate (Kuichling, 1889; Mulvaney, 1851), or via event-based rainfall-runoff models that are able to simulate the full flood hydrograph (Boyd et al., 1996; Chow et al., 1988; Laurenson and Mein, 1997). Regional frequency analysis is one type of method to estimate IDF curves, where the precision of at-site estimates is improved by pooling data from sites in the surrounding region (Hosking and Wallis, 1997). These methods can be combined with spatial interpolation methods to estimate parameters for any ungauged location of interest (Carreau et al., 2013). To determine an effective mean depth of rainfall over a catchment with the same exceedance probability as at a gauge location, the pointwise estimate of extreme rainfall is multiplied by an areal reduction factor (ARF) (Ball et al., 2016). However, such methods do not account for information on the spatial dependence of extreme rainfall—whether for single storm duration, or for the more complex case of different durations across a region (Bernard, 1932; Koutsoyiannis et al., 1998). The lack of dependence prevents these approaches from being applied to estimate conditional or joint flood risk at multiple points in a catchment or across several catchments, as would be required for a civil infrastructure system.

Although multivariate approaches can be tailored to estimate conditional and joint probabilities of extreme rainfall for specific situations (e.g., Kao and Govindaraju (2008), Wang et al. (2010), Zhang and Singh (2007)), the development of a unified methodology that integrates with existing IDF-based flood estimation approaches remains elusive. This is particularly challenging given that it is not only necessary to preserve dependence of rainfall across space, but also to account for dependence across storm burst durations, as different parts of the system may be vulnerable to different critical duration storm events. To this end, max-stable process theory has been demonstrated to represent storm-level dependence (de Haan, 1984; Schlather, 2002) and used to calculate conditional probabilities for a spatial domain (Padoan et al., 2010). Copulas including the extremal-t copula (Demarta and McNeil, 2005), and the Husler-Reiss copula (Hüsler and Reiss, 1989) have also been used to model rainfall dependence.

This study applies a max-stable approach with an emphasis on practical flood estimation problems:

1. The approach needs to account for, not only the spatial dependence of rainfall 'events' of a single duration, but also the dependence across multiple durations. This was addressed by Le et al. (2018b), who linked the max-stable model of Brown and Resnick (1977) with the duration-dependent model of Koutsoyiannis et al. (1998), to create a model that could be used to reflect dependencies between nearby catchments of different sizes.
2. Given that often the interest is in rare flood events, the model needs to capture appropriate asymptotic properties of spatial dependence as the events become increasingly extreme. Recent evidence is emerging that rainfall has an asymptotically independent characteristic (Le et al., 2018a; Thibaud et al., 2013), which means that the level of the rainfall's dependence reduces with an increasing return period (Wadsworth and Tawn, 2012). The requirement of asymptotic independence indicates that inverted max-stable models are preferable over max-stable models.

This study adapts the methods developed by Le et al. (2018b) to inverted max-stable models to derive spatially-dependent IDF curves and ARFs as the basis for transforming rainfall into flood flows. The

approach is demonstrated on a highway system spanning 20 km with five separate bridge crossings, and with the contributing catchment at each crossing having a different time of concentration.

The case study is designed to address two related questions: (i) "What flood flow needs to be used to design a bridge that will fail only once on average every M times (e.g., $M = 10$ for a 10-year event) that a neighbouring catchment is flooded?"; and (ii) "What is the probability that the overall system fails given that each bridge is designed to a specific exceedance probability event (e.g., the 1% annual exceedance probability event)?" The method for resolving these questions represents a new paradigm in which to estimate flood risk for engineering design, by focusing attention on the risk of the entire system, rather than the risk of individual system elements in isolation.

In the remainder of the paper, Section 2 emphasises the need for spatially dependent IDF curves in flood risk design, followed by Section 3 which outlines the case study and data used. Section 4 explains the methodology of the framework, including a method for analysing the spatial dependence of extreme rainfall across different durations. It also includes an algorithm with which to use that information in estimating the conditional and joint probabilities of floods. The results, and a discussion on the behaviour of flood due to the spatial and duration dependence of rainfall extremes, are provided in Section 5. Conclusions and recommendations follow in Section 6.

2. The need for spatially dependent IDF curves in flood risk estimation

The main limitation of conventional methods of flood risk estimation is that they isolate bursts of rainfall and break the dependence structure of extreme rainfall. Figure 1 demonstrates a traditional process of estimating at-site extreme rainfall for two locations (gauge 1, gauge 2) and three durations (1, 3, and 5 hr) (Stedinger et al., 1993). The process first involves extracting the extreme burst of rainfall for each site, duration and year from the continuous rainfall data, and then fitting a probability distribution (such as the Generalised Extreme Value (GEV) distribution) to the extracted data. Figure 1 demonstrates that, through the process of converting the continuous rainfall data to a series of discrete rainfall 'bursts', this process breaks both the dependence with respect to duration and space. Firstly, the duration dependence is broken by extracting each duration separately, whereas for the hypothetical storm in Fig. 1 it is clear that the annual maxima from some of the extreme bursts come

from the same storm. Secondly, the spatial dependence is broken because each site is analysed independently. Again, for the hypothetical storm of Fig. 1 it can be seen that the 5 hr storm has occurred at the same time across the two catchments, and this information is lost in the subsequent probability distribution curves. Lastly, there is cross-dependence in space and duration. For example, the 1 hr extreme from gauge 2 occurs at the same time as the 5 hr extreme from gauge 1. This may be relevant if there are two catchments with times of concentration matching 1 hr and 5 hr respectively, where catchments are neighbouring or nested.

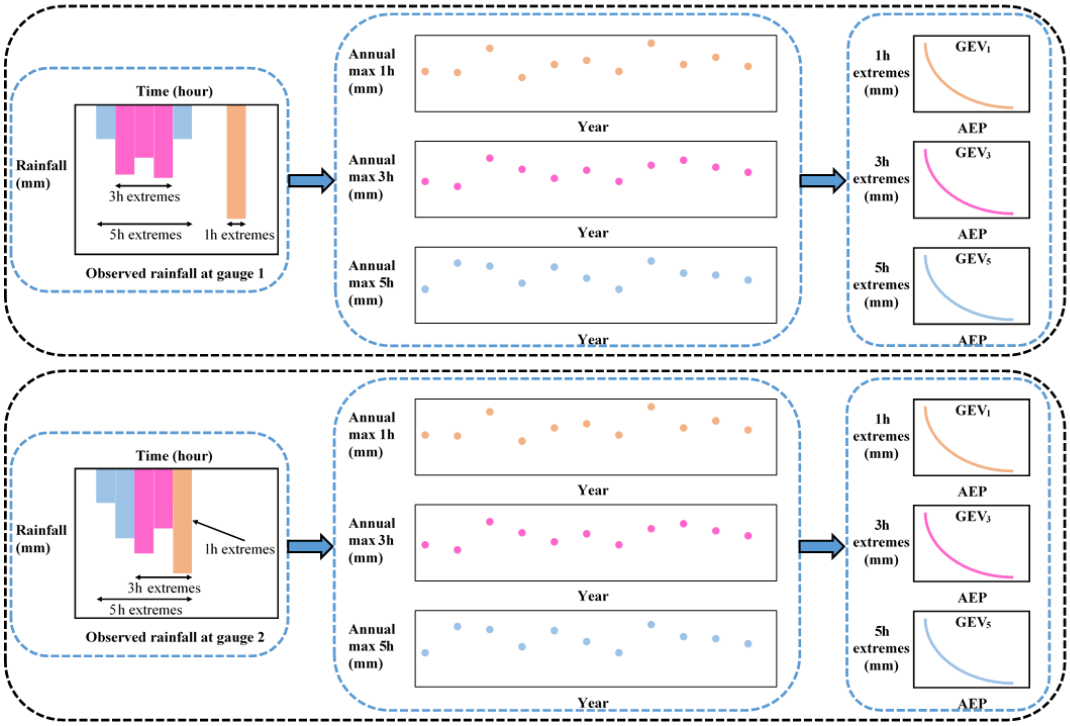

Figure 1. Illustration of process to estimate rainfall extremes for each individual location in conventional flood risk approach, the upper panel is for gauge 1 and the lower panel is for gauge 2.

Having obtained the IDF curves for individual locations in Fig. 1, the next step is commonly to convert this to spatial IDF maps by interpolating results between gauged locations. Figure 2 shows hypothetical IDF curves from individual sites, with a separate spatial contour map usually provided for each storm burst duration. In a conventional application the respective maps are used to estimate the magnitude of extreme rainfall over catchments for a specified time of concentration. The IDF curves are combined with an areal reduction factor (ARF) to determine the volume of rainfall over a region (since rainfall is not simultaneously extreme at all locations over the region). However,

because the spatial dependence was broken in the analysis of IDF curves, the ARF come from a separate analysis and are an attempt to correct for the broken spatial relationship within a catchment (Bennett et al., 2016a). Lastly, the rainfall volume over the catchment is combined with a temporal pattern and input to a runoff model to simulate flood-flow at a catchment's outlet. Where catchment flows can be considered independently this process has been acceptable for conventional design, but because this process does not account for dependence across durations and across a region, it is not possible to address problems that span multiple catchments, as with civil infrastructure systems.

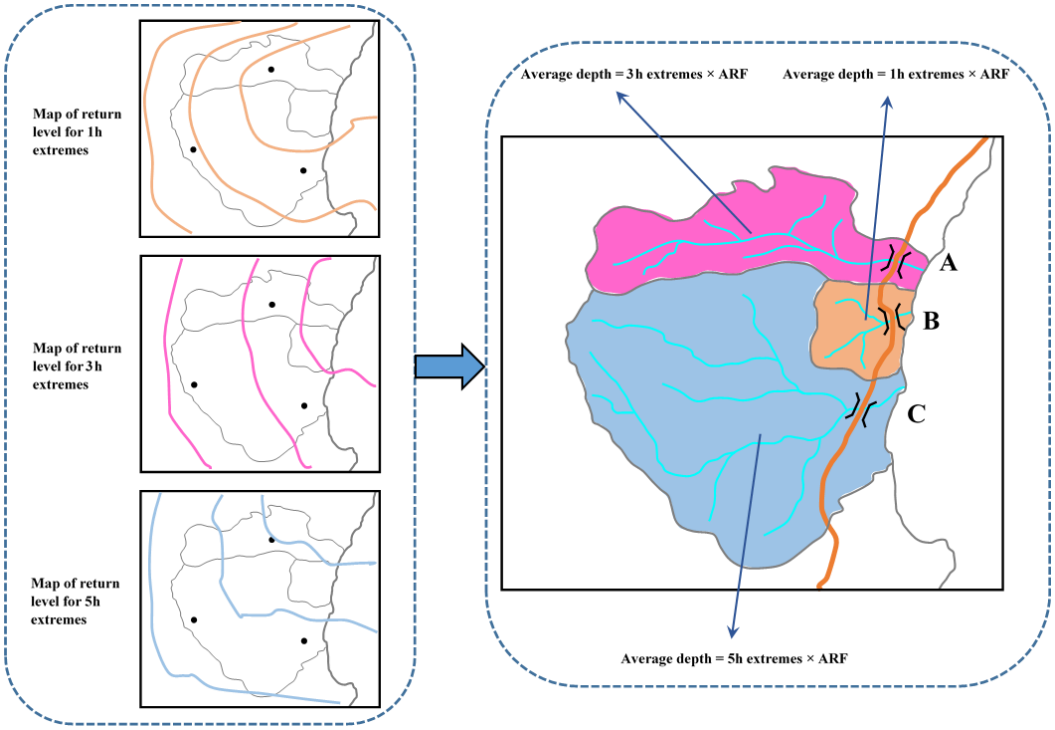

Figure 2. Illustration of map of return level and how to use it in estimating flood flow in conventional flood risk estimates approach.

The process in Fig. 1 breaks out the dependence of the observed rainfall, which makes the conventional approach unable to analyse the dependence of flooding at two or more separate locations. Instead, this paper advocates for spatially dependent IDF curves which are developed by retaining the dependence of observed rainfall in the estimation of extremal rainfall. By applying spatially dependent IDF curves to a rainfall-runoff model, the dependence of flooding between separate locations can be achieved.

3. Case study and data

The region chosen for the case study is in the mid north coast region of New South Wales, Australia. This region has been the focus of a highway upgrade project and has an annual average daily traffic volume on the order of 15,000 vehicles along the existing highway. The upgrade traverses a series of coastal foothills and floodplains for a total length of approximately 20 km. The project's major river crossings consist of extensive floodplains with some marsh areas.

The case study has five main catchments that are numbered in sequence in Fig. 3: (1) Bellinger, (2) Kalang River, (3) Deep Creek, (4) Nambucca and (5) Warrell Creek. The area and time of concentration of these catchments is summarised in Table 1, with the latter estimated using the ratio of the flow path length and average flow velocity (SKM, 2011). The Deep Creek catchment has a time of concentration of 8.3 hr, while the other four catchments have much longer times of concentration, ranging from 27.8 to 38.9 hr. These require the estimates of spatial dependence across different durations of rainfall extremes. Although the spatial dependence across rainfall durations would be expected to be lower than across a single duration, since short- and long-rain events are often driven by different meteorological mechanisms (Zheng et al., 2015), it is nonetheless likely that some level of spatial dependence would exist and need to be integrated into the risk calculations. This is particularly of relevance given extremal rainfall in this region is strongly associated with 'east coast low' systems off the eastern coastline, whereby extreme hourly rainfall bursts are often embedded in heavy multi-day rainfall events.

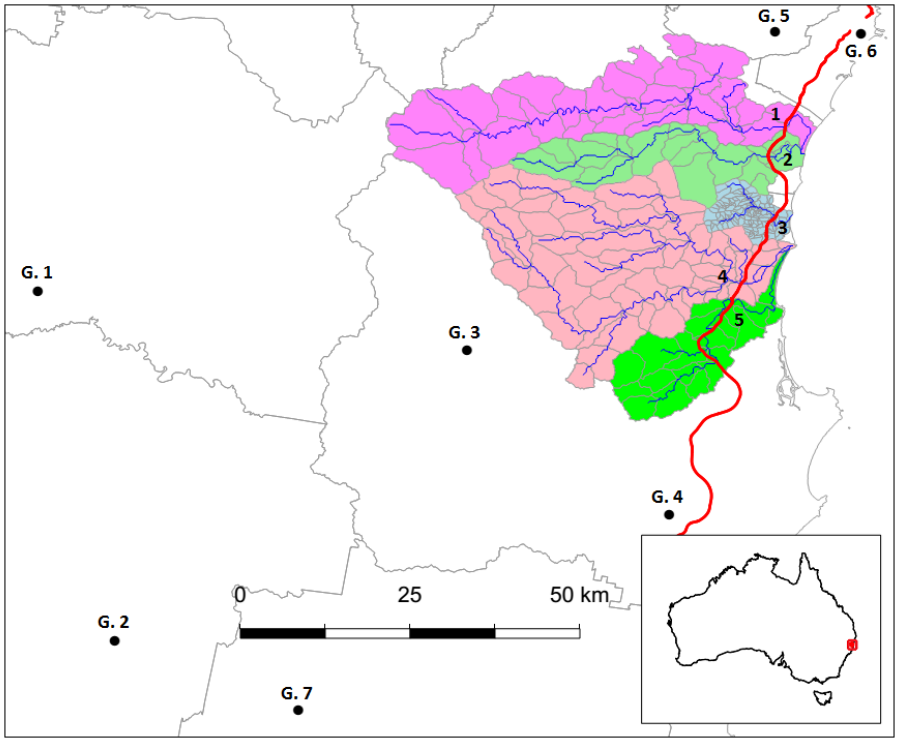

Figure 3. Map of the case study in New South Wales, Australia. The black dots indicate the rainfall gauges (G. 1 to G. 7), the red line indicates the Pacific Highway upgrade project, and the blue lines indicate the main river network. The numbers from one to five indicate the locations of the main river crossings.

Table 1. Summary of properties for catchments in the case study.

No.	Catchment	Area (ha)	Raw time of concentration (hour)
1	Bellinger	77150	37
2	Kalang River	34140	33
3	Deep Creek	9180	8
4	Nambucca (upper)	102015	38
5	Warrell Creek	29440	27

The black circles in Fig. 3 represent the sub-daily rain stations used for this study. There were 7 sub-daily stations selected, with 35 years of record in common for the whole region. The data was available at a 5 minute interval and aggregated to longer durations. For convenience in comparing the times of concentration between the catchments, this study assumes a time of concentration of 9 hr for the Deep Creek catchment, while identical times of concentration of 36 hr are assumed for the other four catchments.

4. Methodology

This section provides the method used to estimate the conditional and joint probabilities of flood for civil infrastructure systems based on rainfall extremes, which is explained according to the steps shown in Fig. 4. First, the generalized Pareto distribution (GPD) is used as marginal distribution to fit to observed rainfall for all duration at each locations (Section 4.1). After that, an inverted max-stable process is introduced and then fitted to rainfall extremes of identical or different durations (Sections 4.2 & 4.3). The conditional and joint probabilities of rainfall are then estimated in Section 4.4, which is followed by the simulation to calculate areal reduction factor (ARF) in Section 4.5. An event-based rainfall-runoff model is employed in Section 4.6 to transform conditional rainfall to conditional flows. With an assumption that there is a one-to-one correspondence between rainfall intensity and flow rate, the joint flood probability for the case study is equal to the joint probability of rainfall. An analysis for the independent model (the case of complete independence) is also implemented for comparison.

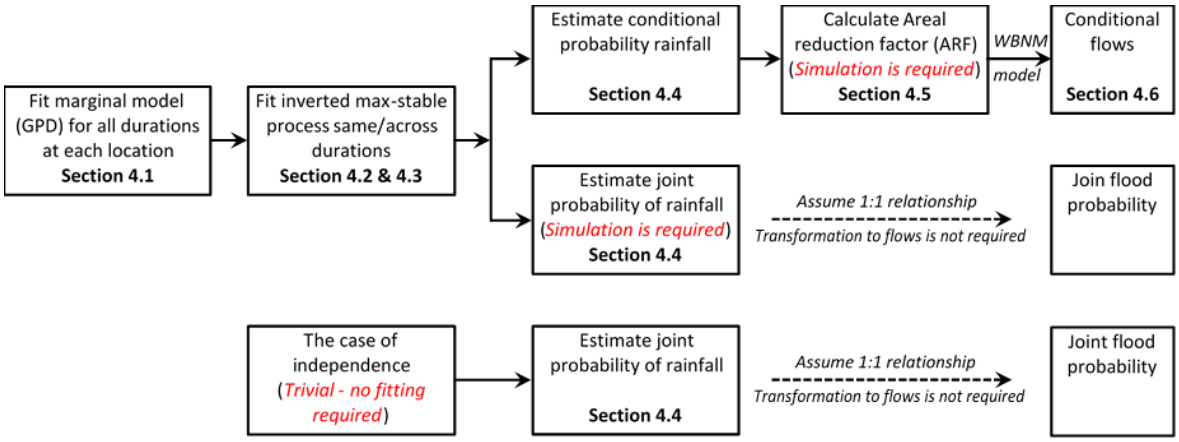

Figure 4. The flow chart for the overall methodology.

4.1. Marginal model for rainfall

This study defines extremes as those greater than some threshold u. For large u, the distribution of Y conditional on $Y > u$ may be approximated by the generalized Pareto distribution (GPD) (Pickands, 1975; Davison and Smith, 1990; Thibaud et al., 2013):

$$G(y) = 1 - \left\{1 + \frac{\xi(y-u)}{\sigma_u}\right\}^{-1/\xi}, \quad y > u, \tag{1}$$

defined on $\{y: 1 + \xi(y-u)/\sigma_u > 0\}$ where $\sigma_u > 0$ and $-\infty < \xi < +\infty$ are scale and shape parameters, respectively. The probability that a level y is exceeded is then $\Phi_u\{1 - G(y)\}$, where $\Phi_u = \Pr(Y > u)$.

The selection of the appropriate threshold u involves a trade-off between bias and variance. A threshold that is too low leads to bias because the GPD approximation is poor. A threshold too high leads to high variance because of a small number of excesses. Two diagnostic tests are used to determine the appropriate threshold u: the mean residual life plot and the parameter estimate plot (Coles, 2001; Davison and Smith, 1990). These methods use the stability property of a GPD, so that if a GPD is valid for all excesses above u, then excesses of a threshold greater than u should also follow a GPD. Detailed guidance of these methods can be found in Coles (2001).

4.2. Dependence model for spatial rainfall

Consider rainfall as a stationary stochastic process Z_i associated with a location x_i in a region of interest (the notation for the stochastic process is simplified from $Z(x_i)$ to Z_i). Without loss of generality it can be assumed that the margins of Z have a unit Fréchet distribution. An important property of dependence in the extremes is whether or not two variables are likely/unlikely to co-occur as the extremes become rarer, as this can significantly influence the estimate of frequency for flood events of large magnitude. This is referred to as asymptotic dependence/independence, respectively. For the case of asymptotic independence, the dependence structure becomes weaker as the extremal threshold increases, which is formally defined as $\lim_{z\to\infty} P\{Z_1 > z | Z_2 > z\} = 0$ for all $x_1 \neq x_2$. The spatial extent of a rainfall event with asymptotically independent extremes will diminish as its rarity increases.

An example of an asymptotically independent model is the inverted max-stable process (Wadsworth and Tawn, 2012). A general description of all continuous inverted max-stable processes that have standard exponential margins on a spatial domain X is

$$\widetilde{\Omega}(x) = \min_{k\geq 1} U_k / W_k, \quad x \in X, \tag{2}$$

where U_k are points of a unit Poisson process on $(0, \infty)$ and the $W_k(x)$ are independent replicas of a continuous, non-negative stochastic process $W(x)$ in the spatial domain X, with $E\{W(x)\} = 1$ for all $x \in X$.

It is convenient to work with a simple inverted max-stable process with unit Fréchet margins, because the marginal distribution can easily be transformed back to the GPD scale. To transform the process $\widetilde{\Omega}(x)$ to unit Fréchet margins, the following transformation is used:

$$\Omega(x) = -\frac{1}{\log\left\{1 - e^{-\widetilde{\Omega}(x)}\right\}}, \quad x \in X, \tag{3}$$

then $\Omega(x)$ is an asymptotically independent process with unit Fréchet margins.

From Eq. (2), different models for W give different inverted max-stable processes. There are two popular and easily-simulated classes of model for the inverted max-stable processes: the Brown-Resnick model (Asadi et al., 2015; Huser and Davison, 2013; Kabluchko et al., 2009; Oesting et al., 2017), and extremal-t model (Opitz, 2013). This study uses the Brown-Resnick form of equations from the family of an inverted max-stable process because Le et al. (2018a) showed it has better performance than the extremal-t model.

4.3. Fitting the dependence model

One simple way to calibrate dependence models is to fit them to data by matching a suitable statistic. The dependence structure of the inverted max-stable process is represented by the pairwise residual tail dependence coefficient (Ledford and Tawn, 1996).

For a generic continuous process Z_i associated with a specific location x_i the empirical pairwise residual tail dependence coefficient η for each pair of locations (x_1, x_2) is

$$\eta(x_1, x_2) = \lim_{y \to \infty} \frac{\log P\{Z_2 > z\}}{\log P\{Z_1 > z, Z_2 > z\}}. \tag{4}$$

The value of $\eta \in (0,1]$ indicates the level of extremal dependence between Z_1 and Z_2 (Coles et al., 1999), with lower values indicating lower dependence. An example of how to calculate the residual tail dependence coefficient is provided in Appendix A for a sample dataset.

To estimate the dependence structure of an inverted max-stable model, the theoretical residual tail dependence coefficient function is usually fitted to its empirical counterpart. Here the residual tail dependence coefficient function is assumed to only depend on the Euclidean distance between two locations $h = \|x_1 - x_2\|$. The theoretical residual tail dependence coefficient function for the inverted Brown-Resnick model is given as:

$$\eta(h) = \frac{1}{2\Phi\left\{\sqrt{\frac{\gamma(h)}{2}}\right\}}, \quad (5)$$

where Φ is the standard normal cumulative distribution function, h is the distance between two locations, and $\gamma(h)$ belongs to the class of variograms $\gamma(h) = \|h\|^{\beta}/q$ for $q > 0$ and $\beta \in (0,2)$. The models are then fitted to the empirical residual tail dependence coefficients by modifying parameters q and β until the sum of squared errors is minimized.

In the case that extreme rainfall at locations x_1 and x_2 are of identical duration (i.e. both 36 hr), then the inverted max-stable process is fitted to the observations by minimizing the sum of the squared errors of the residual tail dependence coefficients. This information can be directly applied to the case where two catchments have a similar time of concentration owing to their similar shape and size. However, there are many instances when two catchments of interest will have differing times of concentration; in particular, when the extreme rainfall at location x_1 and x_2 are of different durations (e.g., 36 hr and 9 hr), the dependence is less than the case of 36 hr and 36 hr. This observation is evident when considering the special case of a single location, i.e. the same point is considered twice, at a distance of $h = 0$. For the case where the duration is the same, the rainfall values are identical and have perfect dependence, but when the duration of extremes are different the values are not identical and the dependence is less. Therefore, an adjustment needs to be made to ensure that the theoretical pairwise residual tail dependence coefficient function suitably represents the observed pairwise residual tail dependence coefficients for the case of extreme rainfalls of different durations.

Following Le et al. (2018b), an adjusted approach is used by adding a nugget to the variograms as:

$$\gamma_{ad.}(h) = h^{\beta}/q + c(D - d)/d, \quad (6)$$

where h, β, and q are the same as those in Eq. (5); d is the duration (in hours); $0 < d \leq D$, where D is the maximum duration of interest (e.g. $D = 36$ hr for the case study described in this paper); and c is a parameters to adjust dependence according to duration. This adjustment is intended to condition the behaviour of shorter duration extremes on a D-hour extreme of a specified magnitude. It is constructed to reflect the fact that when compared to a D-hour extreme, a shorter duration results in less extremal dependence. Cases involving conditioning of longer periods on shorter periods (such as a 36 hr extreme given a 9 hr extreme has occurred) can also use the relationship in Eq. (6), but with different parameter values.

To fit the inverted max-stable process for all pairs of durations at locations x_1 and x_2 (i.e. 36 hr and 12 hr, 36 hr and 9 hr, 36 hr and 6 hr, 36 hr and 2 hr, 36 hr and 1 hr), the theoretical pairwise residual tail dependence coefficient function in Eq. (5) is used with the adjusted variogram from Eq. (6) where the parameters β and q are first obtained from the fitted results of the case of identical 36 hr durations at location x_1 and x_2. The parameter c is obtained by a least square fit of the residual tail dependence coefficient across all durations.

4.4. Estimate of conditional and joint probabilities of rainfall extremes

The conditional probability $P\{Z_2 > z_2 | Z_1 > z_1\}$ is obtained from the bivariate inverted max-stable process cumulative distribution function (CDF) in unit Fréchet margins (Thibaud et al., 2013), which is given as:

$$P\{Z_1 \leq z_1, Z_2 \leq z_2\} = 1 - \exp\left\{-\frac{1}{g_1}\right\} - \exp\left\{-\frac{1}{g_2}\right\} + \exp[-V\{g_1, g_2\}], \qquad (7)$$

where $g_1 = -1/\log\{1 - \exp(-1/z_1)\}$, $g_2 = -1/\log\{1 - \exp(-1/z_2)\}$, and the exponent measure V (Padoan et al., 2010) is defined as:

$$V\{g_1, g_2\} = -\frac{1}{g_1}\Phi\left\{\frac{a}{2} + \frac{1}{a}log\frac{g_2}{g_1}\right\} - \frac{1}{g_2}\Phi\left\{\frac{a}{2} + \frac{1}{a}log\frac{g_1}{g_2}\right\}. \qquad (8)$$

In Eq. (8), Φ is the standard normal cumulative distribution function, $a = \sqrt{2\gamma_{ad.}(h)}$ with $\gamma_{ad.}(h)$ is the variograms that was mentioned in the explanation of Eq. (6).

In unit Fréchet margins, the relationship between the return level z and the return period T is given as $z = -1/log(1 - 1/T)$, and the conditional probability for the max-stable process can then be estimated using:

$$P\{Z_2 > z_2 | Z_1 > z_1\} = T_1 \left[\frac{1}{T_1} - \exp\left(-\frac{1}{z_2}\right) + P\{Z_1 \leq z_1, Z_2 \leq z_2\}\right], \quad (9)$$

where T_1 is the return period corresponding to the return level z_1.

The joint probability for independent variables is broken down as the product of the marginals. The probability that there is at least one location that has an extreme event exceeding a given threshold for the case that all of events are independent can be calculated based on the addition rule for the union of probabilities, as:

$$P(Z_1 > z_1 \text{ or } \dots \text{ or } Z_N > z_N) = \sum_{i=1}^{N} P(Z_i > z_i) - \sum_{i<j} P\left(Z_i > z_i, Z_j > z_j\right) + \cdots$$

$$+(-1)^{N-1} P(Z_1 > z_1, \dots, Z_N > z_N), \quad (10)$$

where $\boldsymbol{N}$ is the number of locations, and $\boldsymbol{P(Z_1 > z_1, \dots, Z_N > z_N) = P(Z_1 > z_1) \dots P(Z_N > z_N)}$, because all of the events are independent.

4.5. Areal reduction factor estimation and simulation procedure for spatial rainfall

Before transforming extreme rainfall to flood flow through an event-based model, areal reduction factors (ARFs) were employed to make the adjustment of rainfall depth at a point (i.e. the centroid of a catchment) for a given return level estimate, to an effective (mean) depth over a catchment with the same probability of exceedance as the single point (Ball et al., 2016; Le et al., 2018a). ARFs can be estimated from observed rainfall data, but it is difficult to extrapolate ARFs for long return periods from observations with just 35 years of record for this study. To deal with this difficulty and to analyse the asymptotic behaviour of ARFs, Le et al. (2018a) proposed a framework to simulate ARFs for long return periods by using an inverted max-stable process, which is applied here for durations of 36 and 9 hrs.

The simulation procedure for spatial rainfall for a given duration is implemented in two steps. In the first step, the theoretical residual tail dependence coefficient function in Eq. (5) is fitted to observed rainfall for the duration of interest to obtain the variogram parameters $q > 0$ and $\beta \in (0,2)$. The Brown-Resnick process with unit Fréchet margins is then simulated using the algorithm of Dombry et al. (2016) over a spatial domain and the inverted Brown-Resnick process with unit Fréchet margins is obtained through Eq. (2) and Eq. (3). In the second step, the simulation in step 1 is transformed from unit Fréchet margins to the rainfall scaled margins. For rainfall magnitudes above the threshold the generalised Pareto distribution in Eq. (1) is used, and below the threshold the empirical distribution is used. The empirical distributions at ungauged sites are derived from the nearest gauged sites using a response surface (latitude and longitude covariates) to spatially interpolate the threshold.

An advantage of this approach is that it can reflect the proportion of dry days in the empirical distribution by making the simulated rainfall contain zero values (Thibaud et al., 2013). Another advantage is that this approach guarantees that the marginal distributions of simulated rainfall below the threshold matches the observed marginal distributions. There may be a drawback of this approach by forcing the simulated rainfall to have the same extremal dependence structure for both parts below and above the threshold, which may not be true for non-extreme rainfall. However, the dependence structure of non-extreme rainfall contributes insignificantly to extreme events (Thibaud et al., 2013) and is unlikely to affect the results.

For calculating ARFs, the simulation is implemented separately for spatial rainfall of 36 and 9 hrs duration. After the simulated spatial rainfall for 36 and 9 hrs are respectively obtained, ARFs are calculated for each duration and different return periods, which can be found in the supplementary material (Fig. S1 and S2). Figure S1 and S2 provide relationships between ARFs and area (in km^2) for different return periods for the case study catchments. These relationships are calculated through the simulation of inverted Brown-Resnick process over equally sized grid points. The relationships are interpolated to obtain the ARFs for each of subcatchments (corresponding to respective areas 91 km^2, 294 km^2, 341 km^2, 771 km^2, 1020 km^2). When the interest is in the joint probability of rainfall extremes of different durations, the simulation of spatial rainfall should be implemented across

multiple durations. In this case, each term of the covariance matrix is calculated from the dependence structure of the corresponding pair of locations. In detail, the covariance matrix of the simulation procedure provided by Dombry et al. (2016) is calculated from the variogram in Eq. (6). The covariance element for a pair of locations with the same duration (e.g. 36 and 36 hr) is calculated from the variogram of identical durations for 36 and 36 hr. The covariance element for a pair of locations with different durations (e.g. 36 and 9 hr) is calculated from the variogram across durations for 36 and 9 hr.

4.6. Transforming rainfall extremes to flood flow

To estimate flood flow from rainfall extremes, the Watershed Bounded Network Model (WBNM) (Boyd et al., 1996), is employed in this study. WBNM calculates flood runoff from rainfall hyetographs that represent the relationship between the rainfall intensity and time (Chow et al., 1988). It divides the catchment into subcatchments, allowing hydrographs to be calculated at various points within the catchment, and allowing the spatial variability of rainfall and rainfall losses to be modelled. It separates overland flow routing from channel routing, allowing changes to either or both of these processes, for example in urbanised catchments. The rainfall extremes are estimated at the centroid of the catchment, and are converted to average spatial rainfall using the simulated ARFs described in Section 4.5 before estimation of the rainfall hyetographs.

Hydrological models (WBNM) for the case study area were developed and calibrated (WMAWater, 2011). Hydrological model layouts for the Bellinger, Kalang River, Nambucca, Warrell and Deep Creek catchments can be found in the supplementary material (Fig. S3 to S5).

5. Results and discussion

5.1. Evaluation of model for space-duration rainfall process

A GPD with an appropriate threshold was fitted to the observed rainfall data for 36 hr and 9 hr durations, and the Brown-Resnick inverted max-stable process model was calibrated to determine the spatial dependence.

Analysis of the rainfall records led to the selection of a threshold of 0.98 for all records as reasonable across the spatial domain and the GPD was fitted to data above the selected threshold. Figure 5 shows QQ plots of the marginal estimates for a representative station for two durations 36 and 9 hr. Overall the quality of fitted distributions is good and plots for all other stations can be found in the supplementary material (Fig. S6 and S7).

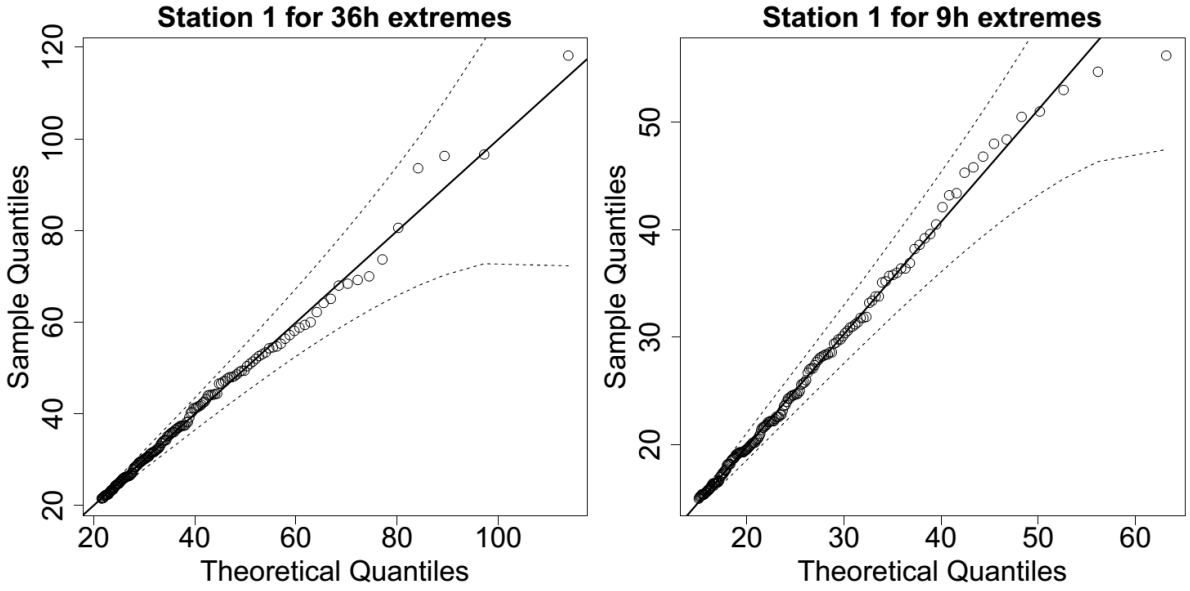

Figure 5. QQ plots for the fitted GPD at one representative station, dotted lines are the 95% confidence bounds, and the solid diagonal line indicates a perfect fit.

The inverted max-stable process across different durations was calibrated to determine dependence parameters. The theoretical pairwise residual tail dependence coefficient function between two locations (x_1 and x_2) was calculated based on Eq. (5) and Eq. (6), and the observed pairwise residual tail dependence coefficient η was calculated using Eq. (4). Figure 6 shows the pairwise residual tail dependence coefficients for the Brown-Resnick inverted max-stable process versus distance. The black points are the observed pairwise residual tail dependence coefficients, while the red lines are the fitted pairwise residual tail dependence coefficient functions. A coefficient equal to 1 indicates complete spatial dependence, and a value of 0.5 indicates complete spatial independence. The top-left panel shows the dependence between 36 hr extremes across space, with the distance $h = 0$ corresponding to "complete dependence". It also shows the dependence decreasing with increasing distance. Figure 6 indicates that the model has a reasonable fit to the observed data given the small

number of dependence parameters. Although the theoretical coefficient (red line) does not perfectly at long distances, the main interest is in short distances, especially at $h = 0$ for the case of dependence between two different durations at the same location.

The remaining panels of Fig. 6 show the dependence of 36 vs. 9 hr extremes, 36 vs. 6 hr extremes, and 36 vs. 3 hr extremes, with the latter two duration combinations not being used directly in the study but nonetheless showing the model performance across several durations. As expected, the dependence levels are weaker compared with 36 vs. 36 hr extremes at the same distance, especially at zero distance. This is expected, as the dependence at the same site between exceedances at different durations will be lower than between exceedances at the same duration. This is because exceedances of different durations may arise from different storm events (Zheng et al., 2015).

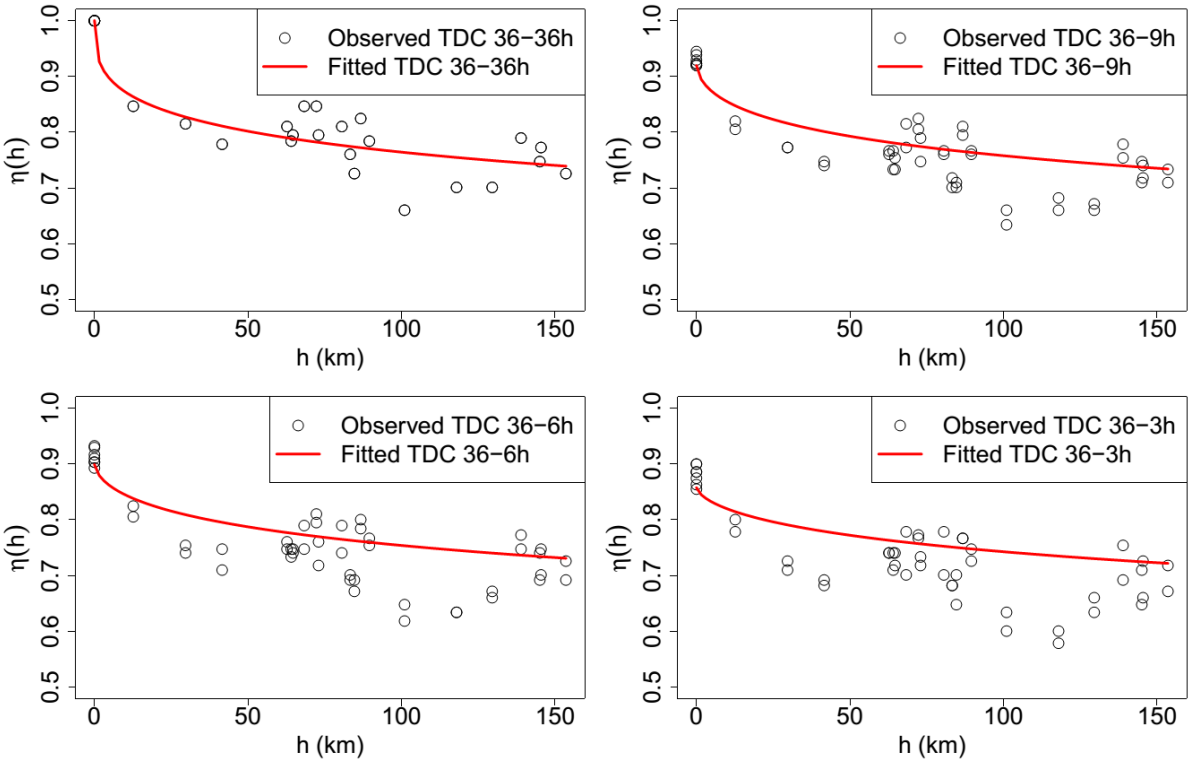

Figure 6. Plots of pairwise residual tail dependence coefficient (TDC) against distance for 36 hr extremes and 36 hr extremes (top left), for 36 hr extremes and 9 hr extremes (top right), for 36 hr extremes and 6 hr extremes (bottom left), and for 36 hr extremes and 3 hr extremes (bottom right). The black points are estimated residual tail dependence coefficients for pairs of sub-daily stations, and the red lines are theoretical residual tail dependence coefficient function.

5.2. Estimating conditional rainfall extremes and corresponding conditional flows for evacuation route design

The recommended approach for estimating conditional rainfall extremes is demonstrated by considering a hypothetical evacuation route across location x_2, given a flood occurs at location x_1, evaluated using Eq. (9). This approach is applied to a case study of the Pacific Highway upgrade project that contains five main river crossings (from Fig. 3). For evacuation purposes, we need to know "what is the probability that a bridge fails only once on average every M times (e.g., $M = 10$ for an one in 10 chance conditional event) that its neighbouring bridge is flooded?" This section provides the conditional estimates for two pairs of neighbouring bridges in the case study that have the shortest Euclidean distances, i.e. pairs (x_1, x_2) and (x_2, x_3). The comparisons of unconditional and conditional maps are given in Fig. 7 and Fig. 8, and the corresponding unconditional and conditional flows are given in Fig. 9. In order to obtain the maps in Fig. 7 and Fig. 8, a thin plate spline regression against longitude and latitude was employed to build the response surface for the marginal distribution parameters of rainfall at every pixel.

The left panel of Fig. 7 provides the pointwise 10-year unconditional return level map over the case study area for 36 hr rainfall extremes. The value at the location of interest—the blue star (the centroid of Bellinger catchment)—is around 260 mm. The right panel of Fig. 7 indicates that when accounting for the effect of a 20-year event for 36 hr rainfall extremes happening at the location of the red star (the centroid of Kalang River catchment), the pointwise one in 10 chance conditional return level at the blue star rises to around 453 mm (i.e., 1.74 times the unconditional value).

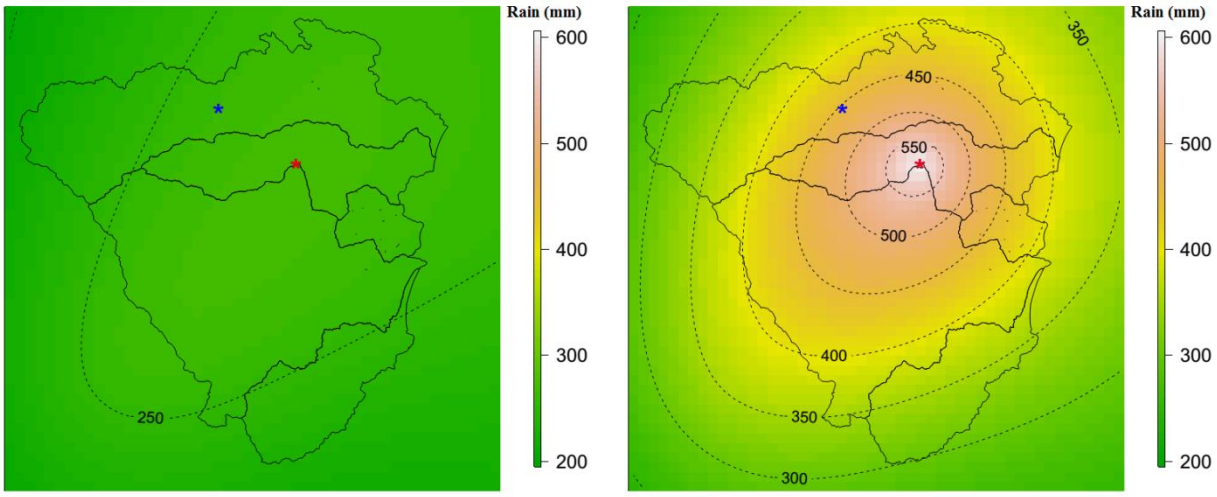

Figure 7. Pointwise 10-year unconditional return level map (mm) for 36 hr extremes (left), and pointwise one in 10 chance conditional return level map (mm) for 36 hr extremes given a 20-year event for 36 hr extremes happen at location of the red star for the centroid of Kalang River catchment (right). The colour scales are the same for comparison.

Figure 8 provides similar plots to Fig. 7 for another pair of locations having different durations of rainfall extremes due to different times of concentration in each catchment. Here, the location of interest is the centroid of the Deep Creek catchment (the blue star in Fig. 8) and the conditional point is the centroid of the Kalang River catchment (the red star in Fig. 8). The pointwise 10-year unconditional and one in 10 chance conditional return levels at the location of the blue star are 134 mm and 194 mm, respectively. The relative difference between the conditional and unconditional return levels is only 1.45 times, compared with 1.74 times for the case in Fig. 7. This is because the pair of locations in Fig. 8 has a longer distance than those in Fig. 7, so that the dependence level is weaker. Moreover, the location pair in Fig. 8 was analysed for different durations (between 36 and 9 hr extremes), which has weaker dependence than the case of the equivalent durations in Fig. 7 (between 36 and 36 hr), based on Fig. 6.

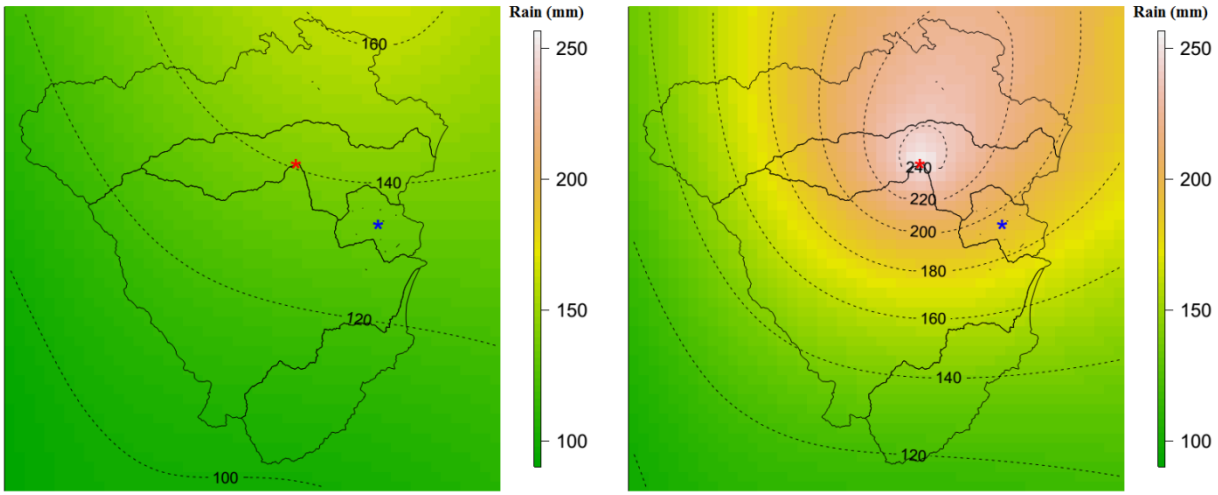

462

463 **Figure 8.** Pointwise 10-year unconditional return level map (mm) for 9 hr extremes (left), and pointwise one in 10 chance
464 conditional return level map (mm) for 9 hr extremes, given a 20-year event for 36 hr extremes happens at location of the red
465 star for the centroid of the Kalang River catchment (right). The colour scales are the same for comparison.

466 The unconditional and conditional return levels are transformed to flood flows via the hydrological
467 model WBNM previously calibrated to each catchment (WMAWater, 2011). The unconditional and
468 conditional return levels were extracted at the centroid of each main catchment, which were then
469 converted to the average spatial rainfall using an areal reduction factor (ARF). The corresponding
470 unconditional and conditional flood flows at the river crossing in the Bellinger catchment
471 (corresponding to the unconditional and conditional rainfall extremes in Fig. 7) are given in Fig. 9
472 (left panel). Similar plots for the river crossing in the Deep Creek catchment (corresponding to the
473 unconditional and conditional rainfall extremes in Fig. 8) are given in Fig. 9 (right panel).

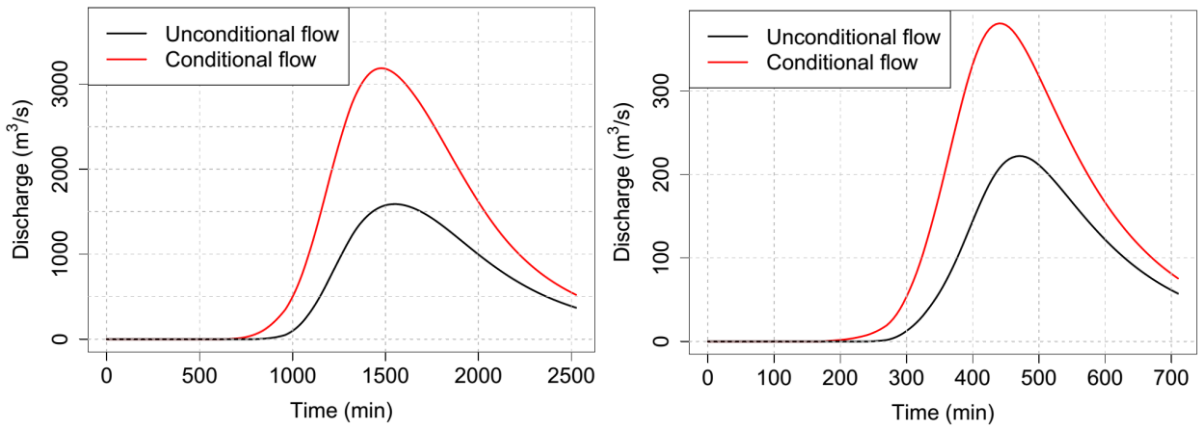

474

Figure 9. Comparison between conditional flows (red line) and unconditional flows (black line). (left) At the river crossing in the Bellinger catchment (number 1 in Figure 3): conditional flow caused by an one in 10 chance conditional event for 36 hr rainfall in considering the effect of a 20-year event for 36 hr rainfall occurring at the river crossing in the Kalang River catchment, and unconditional flow caused by a 10-year unconditional event for 36 hr. (right) At the river crossing in the Deep Creek catchment (number 3 in Figure 3): conditional flow caused by an one in 10 chance conditional event for 9 hr rainfall in considering the effect of a 20-year event for 36 hr rainfall occurring at the river crossing in the Kalang River catchment, and unconditional flow caused by a 10-year unconditional event for 9 hr rainfall.

The left panel of Fig. 9 indicates that the peak conditional flow at the river crossing in the Bellinger catchment is almost 2.0 times higher than that for unconditional flow. The time taken to reach to the peaks is the same for both cases. This is because this river crossing is affected by a large region with a long time of concentration (36 hr); the impact of rainfall losses on the hydrograph is insignificant. This difference is a direct result of the conditional relationship being more stringent than the unconditional relationship. Given that there is an existing extreme event nearby, it is more likely for an extreme event to occur at another location of interest in the region. If a bridge design were to take into account this extra criterion for the purposes of evacuation planning it would require the design to be at a higher level.

Shown in the right panel in Fig. 9, the peak of the conditional flow at the river crossing in the Deep Creek catchment occurred earlier, and is around 1.7 times higher than that for the unconditional flow. This is due to the fact that the river crossing in Deep Creek covers a small region with a short time of concentration (9 hr) and the impact of rainfall losses on the hydrograph is significant. Although Fig. 9 shows a difference in terms of the time taken to reach the peak flows, the two design hydrographs are separate and this is not a physical timing difference.

5.3. Estimating the failure probability of the highway section based on the joint probability of rainfall extremes

The recommended approach for estimating the overall failure probability of a system is demonstrated by considering a hypothetical traffic system with multiple river crossings at locations $x_1, \ldots, x_N$. If there is a one-to-one correspondence between extreme rainfall intensity over a catchment and flood magnitude, the overall failure probability will be approximately equal to the probability that there is at

503 least one river crossing whose contributing catchment has rainfall extremes exceeding the design
504 level, which can be estimated using a large number of simulations from the spatial rainfall model.
505 This approach is applied to the Pacific Highway upgrade project containing five river crossings. A set
506 of 10,000 year simulated rainfall (Section 4.5) is generated from the fitted model (Section 5.1) to
507 calculate the overall failure probability of the highway section. This process is repeated 100 times to
508 estimate the average failure probability, under the assumption that all river crossings are designed to
509 the same individual failure probability.

510 Figure 10 is a plot of the overall failure probability of the highway as a function of the failure
511 probability of each individual river crossing (black). Similar relationships for the cases of complete
512 dependence (blue) and complete independence (red) are also provided for comparison. For the case of
513 complete dependence, when the whole region is extreme at the same time, the overall failure
514 probability of the highway is equal to the individual river crossing failure probability and it represents
515 the best case (the lowest overall failure probability). The worst case is complete independence where
516 extremes do not happen together unless by random chance; this means the failure probability of the
517 highway is much higher than that for individual river crossings. Taking into account the real
518 dependence, there are some extremes that align and it seems from the Fig. 10 that this is a relatively
519 weak effect. As an example from Fig. 10, to design the highway with a failure probability of 1% AEP,
520 we would have to design each individual river crossing to a much rarer AEP of 0.25% (see green lines
521 in Fig. 10).

522

523

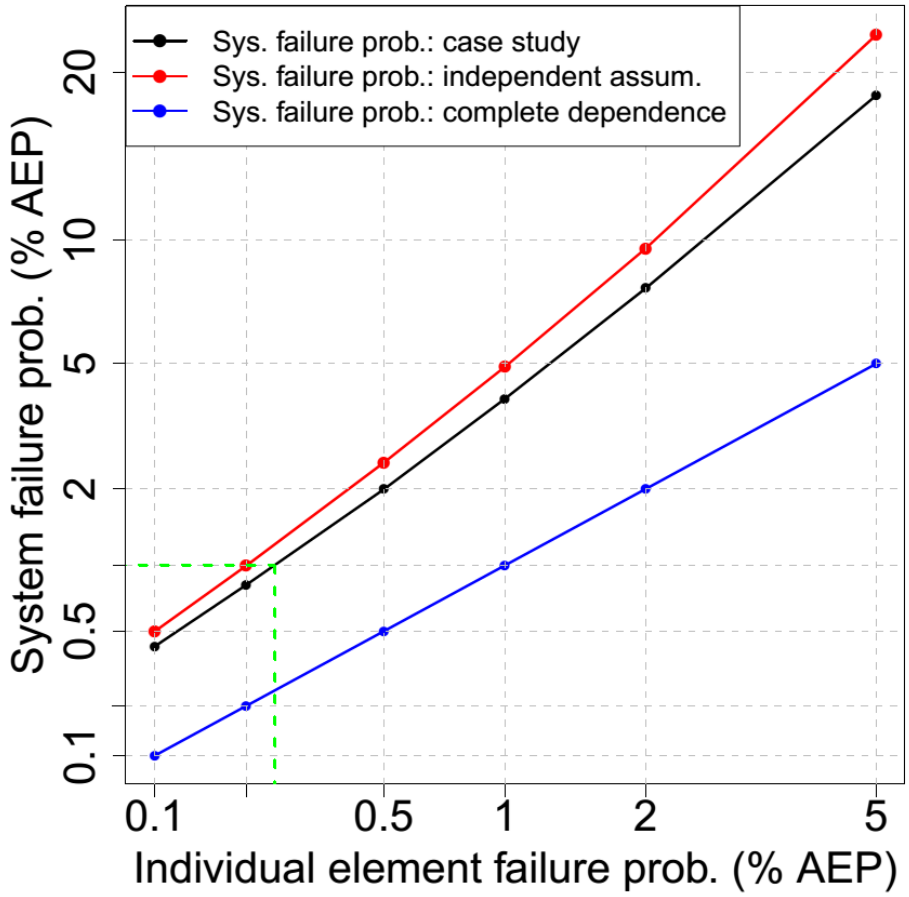

Figure 10. Relationship between system failure probability and individual element failure probability in % annual exceedance probability (% AEP). The black colour is for the case study, the red colour is for the case of complete independence, and the blue is for the case of complete dependence. The green lines help to interpolate the individual element failure probability from a given system failure probability of 1%. Both horizontal axis and vertical axis are constructed at a double log scale for viewing purposes.

6. Discussion and Conclusions

Hydrological design, that is based on IDF curves, has conventionally focussed on individual catchments and individual extremes. Such an approach can lead to an underestimation of wider system risk of flooding since weather systems exhibit dependence in space and time, which can lead to the coincidence of extremes. A number of methods have been developed to address the problem of antecedent moisture within a single catchment, by accounting for the temporal dependence of rainfall at locations of interest through loss parameters or sampling rainfall patterns (Rahman et al., 2002). However, there have been fewer methods that account for the spatial dependence of rainfall across multiple catchments, due in part to the complexity of representing the effects of spatial dependence in

risk calculations. Different catchments can have different times of concentration, so spatial dependence may also imply the need to consider dependence across different durations of extreme rainfall bursts.

Recent and ongoing advances in modelling spatial rainfall extremes provide an opportunity to revisit the scope of hydrological design. Such models include a max-stable model fitted using a Bayesian hierarchical approach (Stephenson et al., 2016), max-stable and inverted max-stable models (Nicolet et al., 2017; Padoan et al., 2010; Russell et al., 2016; Thibaud et al., 2013; Westra and Sisson, 2011) and latent-variable Gaussian models (Bennett et al., 2016b). The ability to simulate rainfall over a region means that hydrological problems need not be confined to individual catchments, but may cover multiple catchments. Civil infrastructure systems such as highways, railways or levees are such examples, since the failure of any one element may lead to overall failure of the system. Alternatively, where there is a network, the failure of one element may have implications for the overall system to accommodate the loss, by considering alternative routes. With models of spatial dependence and duration dependence of extremes there is a new and improved ability to address these problems explicitly as part of the design methodology.

This paper demonstrated an application for evaluating conditional and joint probabilities of flood at different locations. This was achieved with two examples: (i) the design of a river crossing that will fail once on average every M times given that its neighbouring river crossing is flooded; and (ii) estimating the probability that a highway section, which contains multiple river crossings, will fail based on the failure probability of each individual river crossing. Due to the lack of continuous streamflow data and subdaily limitations of rain-based continuous simulation, this study used an event-based method of conditional and joint rainfall extremes to estimate the corresponding conditional and joint flood flows. The spatial rainfall was simulated using an asymptotically independent model, which was then used to estimate conditional and joint rainfall extremes. An empirical method was obtained from the framework of Le et al. (2018b) to make an asymptotically independent model—the inverted max-stable process—able to capture the spatial dependence of rainfall extremes across different durations. The fitted residual tail dependence coefficient function

showed that the model can capture the dependence for different pairs of durations. For our example, the highest ratio of the one in 10 chance conditional event (in considering the effect of a 20-year event rainfall occurring at the conditional location) to the 10-year unconditional event was 1.74, for the two catchments having the strongest dependence (Fig. 7). The corresponding conditional flows were then estimated using a hydrological model WBNM and shown to be strongly related to the ratio of conditional and unconditional rainfall extremes (Fig. 9).

The joint probability of rainfall extremes for all catchments and for all possible pairs of catchments in the case study area was estimated empirically from a set of 10,000 years of simulated rainfall extremes, repeated 100 times to estimate the average value. The results showed that there were differences in the failure probability of the highway after taking into account the rainfall dependence, but the effect was not as emphatic as with the case of conditional probabilities. The difference in the failure probability became weaker as the return period increased, which is consistent with the characteristic of asymptotically independent data (Ledford and Tawn, 1996; Wadsworth and Tawn, 2012). A relationship was demonstrated (Fig. 10) to show how the design of the overall system to a given failure probability requires the design of each individual river crossing to a rarer extremal level than when each crossing is considered in isolation. For the case study example, it would be necessary to design each bridge to a 0.25% AEP event in order to obtain a system failure probability of 1%.

There is a need to reimagine the role of intensity-duration-frequency curves. Conventionally they have been developed as maps of the marginal rainfall in a point-wise manner for all locations and for a range of frequencies and durations. The increasing sophistication of mathematical models for extremes, computational power and interactive graphics abilities of online mapping platforms means that analysis of hydrological extremes could significantly expand in scope. With an underlying model of spatial and duration dependence between the extremes, it is not difficult to conceive of digital maps that dynamically transform from the marginal representation of extremes to the corresponding representation conditional extremes after any number of conditions are applied. This transformation is exemplified by the differences between left and right panels in Fig. 7 and Fig. 8. Enhanced IDF maps

would enable a very different paradigm of design flood risk estimation, breaking away from analysing individual system elements in isolation to emphasize the behaviour of entire system.

Appendix A. Calculation of empirical tail dependence coefficient

To illustrate how Eq. (4) in the manuscript is calculated, consider a set of $n = 10$ observed values at the two locations: Z_1 and Z_2 (see Table A1). First, Z_1 and Z_2 are converted to empirical cumulative probability estimates via the Weibull plotting position formula $P = j/(n+1)$ where j is ranked index of a data point giving P_1 and P_2 (see Table A1).

Table A1. Observed data Z_1 and Z_2 and corresponding empirical cumulative probabilities P_1 and P_2.

$\boldsymbol{Z_1}$	$\boldsymbol{Z_2}$	$\boldsymbol{P_1}$	$\boldsymbol{P_2}$
5	10	0.455	0.909
9	1	0.818	0.091
1	7	0.091	0.636
2	6	0.182	0.545
10	4	0.909	0.364
3	3	0.273	0.273
8	9	0.727	0.818
6	2	0.545	0.182
4	8	0.364	0.727
7	5	0.636	0.455

Assume that interest is in values above a threshold $u = 0.5$, in other words, $P\{Z_2 > z\} = P\{P_2 > u\} = 0.5$. In this case we have only one pair, at the index of 7, that satisfy both P_1 and P_2 are greater than $u = 0.5$, thus $P\{Z_1 > z, Z_2 > z\} = P\{P_1 > u, P_2 > u\} = 1/10 = 0.1$. The calculation of the empirical tail dependence coefficient is then

$$\eta(x_1, x_2) = \frac{\log P\{Z_2 > z\}}{\log P\{Z_1 > z, Z_2 > z\}} = \frac{\log P\{P_2 > u\}}{\log P\{P_1 > u, P_2 > u\}} = \frac{\log(0.5)}{\log(0.1)} = 0.301. \qquad (A.1)$$

Acknowledgments

The lead author was supported by the Australia Awards Scholarships (AAS) from Australia Government. A/Prof Westra was supported by Australian Research Council Discovery grant DP150100411. We thank Mark Babister and Isabelle Testoni of WMA Water for providing the hydrologic models for the case study; and Leticia Mooney for her editorial help in improving this manuscript. The rainfall data used in this study were provided by the Australian Bureau of Meteorology, and can be obtained from the corresponding author.

References

Asadi, P., Davison, A. C., and Engelke, S.: Extremes on river networks, Ann. Appl. Stat., 9, 2023-2050, 10.1214/15-AOAS863, 2015.

Ball, J., Babister, M., Nathan, R., Weeks, W., Weinmann, E., Retallick, M., and Testoni, I.: Australian Rainfall and Runoff: A Guide to Flood Estimation, © Commonwealth of Australia (Geoscience Australia), 2016.

Bárdossy, A., and Pegram, G. G. S.: Copula based multisite model for daily precipitation simulation, Hydrol. Earth Syst. Sci., 13, 2299-2314, 10.5194/hess-13-2299-2009, 2009.

Baxevani, A., and Lennartsson, J.: A spatiotemporal precipitation generator based on a censored latent Gaussian field, Water Resources Research, 51, 4338-4358, doi:10.1002/2014WR016455, 2015.

Bennett, B., Lambert, M., Thyer, M., Bates, B. C., and Leonard, M.: Estimating Extreme Spatial Rainfall Intensities, Journal of Hydrologic Engineering, 21, 04015074, doi:10.1061/(ASCE)HE.1943-5584.0001316, 2016a.

Bennett, B., Thyer, M., Leonard, M., Lambert, M., and Bates, B.: A comprehensive and systematic evaluation framework for a parsimonious daily rainfall field model, Journal of Hydrology, https://doi.org/10.1016/j.jhydrol.2016.12.043, 2016b.

Bernard, M. M.: Formulas for rainfall intensities of long duration, Transactions of the American Society of Civil Engineers, 96, 592-606, 1932.

Boughton, W., and Droop, O.: Continuous simulation for design flood estimation—a review, Environmental Modelling & Software, 18, 309-318, https://doi.org/10.1016/S1364-8152(03)00004-5, 2003.

Boyd, M. J., Rigby, E. H., and VanDrie, R.: WBNM — a computer software package for flood hydrograph studies, Environmental Software, 11, 167-172, https://doi.org/10.1016/S0266-9838(96)00042-1, 1996.

Brown, B. M., and Resnick, S. I.: Extreme Values of Independent Stochastic Processes, Journal of Applied Probability, 14, 732-739, 10.2307/3213346, 1977.

Cameron, D. S., Beven, K. J., Tawn, J., Blazkova, S., and Naden, P.: Flood frequency estimation by continuous simulation for a gauged upland catchment (with uncertainty), Journal of Hydrology, 219, 169-187, https://doi.org/10.1016/S0022-1694(99)00057-8, 1999.

Carreau, J., Neppel, L., Arnaud, P., and Cantet, P.: Extreme Rainfall Analysis at Ungaug ed Sites in the South of France : Comparison of Three Approaches, Jour nal de la Société Française de Statistique, 154 No. 2, 119-138, 2013.

Chow, V. T., Maidment, D. R., and Mays, L. W.: Applied Hydrology, McGraw-Hill, c1988, New York, 1988.

Coles, S., Heffernan, J., and Tawn, J.: Dependence Measures for Extreme Value Analyses, Extremes, 2, 339-365, 10.1023/a:1009963131610, 1999.

Coles, S.: An Introduction to Statistical Modeling of Extreme Values, Springer Series in Statistics, Springer, 2001.

Davison, A. C., and Smith, R. L.: Models for exceedances over high thresholds, Journal of the Royal Statistical Society. Series B (Methodological), 393-442, 1990.

de Haan, L.: A Spectral Representation for Max-stable Processes, The Annals of Probability, 12, 1194-1204, 10.2307/2243357, 1984.

Demarta, S., and McNeil, A. J.: The t Copula and Related Copulas, International Statistical Review / Revue Internationale de Statistique, 73, 111-129, 2005.

Dombry, C., Engelke, S., and Oesting, M.: Exact simulation of max-stable processes, Biometrika, 103, 303-317, 2016.

Durocher, M., Chebana, F., and Ouarda, T. B. M. J.: On the prediction of extreme flood quantiles at ungauged locations with spatial copula, Journal of Hydrology, 533, 523-532, https://doi.org/10.1016/j.jhydrol.2015.12.029, 2016.

Favre, A. C., Adlouni, S. E., Perreault, L., Thiémonge, N., and Bobée, B.: Multivariate hydrological frequency analysis using copulas, Water Resources Research, 40, doi:10.1029/2003WR002456, 2004.

Gupta, A. S., and Tarboton, D. G.: A tool for downscaling weather data from large-grid reanalysis products to finer spatial scales for distributed hydrological applications, Environmental Modelling & Software, 84, 50-69, https://doi.org/10.1016/j.envsoft.2016.06.014, 2016.

He, Y., Bárdossy, A., and Zehe, E.: A review of regionalisation for continuous streamflow simulation, Hydrology and Earth System Sciences, 15, 3539, 2011.
Hegnauer, M., Beersma, J., Van den Boogaard, H., Buishand, T., and Passchier, R.: Generator of Rainfall and Discharge Extremes (GRADE) for the Rhine and Meuse basins; Final report of GRADE 2.0, Document extern project, 2014.
Hosking, J. R. M., and Wallis, J. R.: Regional Frequency Analysis - An Approach Based on L-Moments, Cambridge University Press, Cambridge, UK, 1997.
Huser, R., and Davison, A. C.: Composite likelihood estimation for the Brown–Resnick process, Biometrika, 100, 511-518, 10.1093/biomet/ass089, 2013.
Hüsler, J., and Reiss, R.-D.: Maxima of normal random vectors: Between independence and complete dependence, Statistics & Probability Letters, 7, 283-286, https://doi.org/10.1016/0167-7152(89)90106-5, 1989.
Kabluchko, Z., Schlather, M., and de Haan, L.: Stationary Max-Stable Fields Associated to Negative Definite Functions, The Annals of Probability, 37, 2042-2065, 2009.
Kao, S.-C., and Govindaraju, R. S.: Trivariate statistical analysis of extreme rainfall events via the Plackett family of copulas, Water Resources Research, 44, doi:10.1029/2007WR006261, 2008.
Kleiber, W., Katz, R. W., and Rajagopalan, B.: Daily spatiotemporal precipitation simulation using latent and transformed Gaussian processes, Water Resources Research, 48, doi:10.1029/2011WR011105, 2012.
Koutsoyiannis, D., Kozonis, D., and Manetas, A.: A mathematical framework for studying rainfall intensity-duration-frequency relationships, Journal of Hydrology, 206, 118-135, http://dx.doi.org/10.1016/S0022-1694(98)00097-3, 1998.
Kuichling, E.: The relation between the rainfall and the discharge of sewers in populous districts, Transactions of the American Society of Civil Engineers, 20, 1-56, 1889.
Laurenson, E. M., and Mein, R. G.: RORB Version 4 Runoff Routing Program User Manual, Monash University Department of Civil Engineering, 1997.
Le, P. D., Davison, A. C., Engelke, S., Leonard, M., and Westra, S.: Dependence properties of spatial rainfall extremes and areal reduction factors, Journal of Hydrology, 565, 711-719, https://doi.org/10.1016/j.jhydrol.2018.08.061, 2018a.
Le, P. D., Leonard, M., and Westra, S.: Modeling Spatial Dependence of Rainfall Extremes Across Multiple Durations, Water Resources Research, 54, 2233-2248, doi:10.1002/2017WR022231, 2018b.
Ledford, A. W., and Tawn, J. A.: Statistics for Near Independence in Multivariate Extreme Values, Biometrika, 83, 169-187, 1996.
Leonard, M., Lambert, M. F., Metcalfe, A. V., and Cowpertwait, P. S. P.: A space-time Neyman–Scott rainfall model with defined storm extent, Water Resources Research, 44, doi:10.1029/2007WR006110, 2008.
Leonard, M., Westra, S., Phatak, A., Lambert, M., Hurk, B. v. d., McInnes, K., Risbey, J., Schuster, S., Jakob, D., and Stafford-Smith, M.: A compound event framework for understanding extreme impacts, Wiley Interdisciplinary Reviews: Climate Change, 5, 113-128, doi:10.1002/wcc.252, 2014.
Mulvaney, T. J.: On the use of self-registering rain and flood gauges in making observation of the relation of rainfall and floods discharges in a given catchment, Proc. Civ. Eng. Ireland, 4, 18–31, 1851.
Nicolet, G., Eckert, N., Morin, S., and Blanchet, J.: A multi-criteria leave-two-out cross-validation procedure for max-stable process selection, Spatial Statistics, 22, 107-128, https://doi.org/10.1016/j.spasta.2017.09.004, 2017.
Oesting, M., Schlather, M., and Friederichs, P.: Statistical post-processing of forecasts for extremes using bivariate Brown-Resnick processes with an application to wind gusts, Extremes, 20, 309-332, 10.1007/s10687-016-0277-x, 2017.
Opitz, T.: Extremal t processes: Elliptical domain of attraction and a spectral representation, Journal of Multivariate Analysis, 122, 409-413, https://doi.org/10.1016/j.jmva.2013.08.008, 2013.
Padoan, S. A., Ribatet, M., and Sisson, S. A.: Likelihood-Based Inference for Max-Stable Processes, Journal of the American Statistical Association, 105, 263-277, 10.1198/jasa.2009.tm08577, 2010.
Pathiraja, S., Westra, S., and Sharma, A.: Why continuous simulation? The role of antecedent moisture in design flood estimation, Water Resources Research, 48, doi:10.1029/2011WR010997, 2012.

721 Pickands, J.: Statistical Inference Using Extreme Order Statistics, The Annals of Statistics, 3, 119-
722 131, 10.2307/2958083, 1975.
723 Rahman, A., Weinmann, P. E., Hoang, T. M. T., and Laurenson, E. M.: Monte Carlo simulation of
724 flood frequency curves from rainfall, Journal of Hydrology, 256, 196-210,
725 https://doi.org/10.1016/S0022-1694(01)00533-9, 2002.
726 Rasmussen, P. F.: Multisite precipitation generation using a latent autoregressive model, Water
727 Resources Research, 49, 1845-1857, doi:10.1002/wrcr.20164, 2013.
728 Renard, B., and Lang, M.: Use of a Gaussian copula for multivariate extreme value analysis: Some
729 case studies in hydrology, Advances in Water Resources, 30, 897-912,
730 http://dx.doi.org/10.1016/j.advwatres.2006.08.001, 2007.
731 Requena, A. I., Chebana, F., and Ouarda, T. B. M. J.: A functional framework for flow-duration-curve
732 and daily streamflow estimation at ungauged sites, Advances in Water Resources, 113, 328-340,
733 https://doi.org/10.1016/j.advwatres.2018.01.019, 2018.
734 Russell, B. T., Cooley, D. S., Porter, W. C., and Heald, C. L.: Modeling the spatial behavior of the
735 meteorological drivers' effects on extreme ozone, Environmetrics, 27, 334-344, doi:10.1002/env.2406,
736 2016.
737 Schlather, M.: Models for Stationary Max-Stable Random Fields, Extremes, 5, 33-44,
738 10.1023/A:1020977924878, 2002.
739 Seneviratne, S. I., Nicholls, N., Easterling, D., Goodess, C. M., Kanae, S., Kossin, J., Luo, Y.,
740 Marengo, J., McInnes, K., and Rahimi, M.: Managing the Risks of Extreme Events and Disasters to
741 Advance Climate Change Adaptation: Changes in Climate Extremes and their Impacts on the Natural
742 Physical Environment, 2012.
743 Nambucca Heads Flood Study:
744 http://www.nambucca.nsw.gov.au/cp_content/resources/16152_2011__Nambucca_Heads_Flood_Stu
745 dy_Final_Draft_Chapter_6a.pdf, 2011.
746 Stedinger, J., Vogel, R., and Foufoula-Georgiou, E.: Frequency Analysis of Extreme Events, in:
747 Handbook of Hydrology, edited by: Maidment, D. R., McGraw-Hill, New York, 18.11-18.66, 1993.
748 Stephenson, A. G., Lehmann, E. A., and Phatak, A.: A max-stable process model for rainfall extremes
749 at different accumulation durations, Weather and Climate Extremes, 13, 44-53,
750 https://doi.org/10.1016/j.wace.2016.07.002, 2016.
751 Thibaud, E., Mutzner, R., and Davison, A. C.: Threshold modeling of extreme spatial rainfall, Water
752 Resources Research, 49, 4633-4644, 10.1002/wrcr.20329, 2013.
753 Wadsworth, J. L., and Tawn, J. A.: Dependence modelling for spatial extremes, Biometrika, 99, 253-
754 272, 10.1093/biomet/asr080, 2012.
755 Wang, Q. J.: A Bayesian Joint Probability Approach for flood record augmentation, Water Resources
756 Research, 37, 1707-1712, 10.1029/2000WR900401, 2001.
757 Wang, Q. J., Robertson, D. E., and Chiew, F. H. S.: A Bayesian joint probability modeling approach
758 for seasonal forecasting of streamflows at multiple sites, Water Resources Research, 45,
759 doi:10.1029/2008WR007355, 2009.
760 Wang, X., Gebremichael, M., and Yan, J.: Weighted likelihood copula modeling of extreme rainfall
761 events in Connecticut, Journal of Hydrology, 390, 108-115,
762 http://dx.doi.org/10.1016/j.jhydrol.2010.06.039, 2010.
763 Westra, S., and Sisson, S. A.: Detection of non-stationarity in precipitation extremes using a max-
764 stable process model, Journal of Hydrology, 406, 119-128,
765 http://dx.doi.org/10.1016/j.jhydrol.2011.06.014, 2011.
766 WMAWater: Review of Bellinger, Kalang and Nambucca River Catchments Hydrology, Bellingen
767 Shire Council, Nambucca Shire Council, New South Wales Government, 2011.
768 Zhang, L., and Singh, V. P.: Gumbel–Hougaard Copula for Trivariate Rainfall Frequency
769 Analysis, Journal of Hydrologic Engineering, 12, 409-419, doi:10.1061/(ASCE)1084-
770 0699(2007)12:4(409), 2007.
771 Zheng, F., Westra, S., and Leonard, M.: Opposing local precipitation extremes, Nature Clim. Change,
772 5, 389-390, 10.1038/nclimate2579

773 http://www.nature.com/nclimate/journal/v5/n5/abs/nclimate2579.html#supplementary-information,
774 2015.

775 Zscheischler, J., Westra, S., van den Hurk, B. J. J. M., Seneviratne, S. I., Ward, P. J., Pitman, A.,
776 AghaKouchak, A., Bresch, D. N., Leonard, M., Wahl, T., and Zhang, X.: Future climate risk from
777 compound events, Nature Climate Change, 8, 469-477, 10.1038/s41558-018-0156-3, 2018.

778